Journal of Materials Chemistry C

ROYAL SOCIETY OF CHEMISTRY

PAPER

View Article Online
View Journal | View Issue

Cite this: J. Mater. Chem. C, 2024, 12, 12026

A highly transparent and efficient luminescent solar concentrator based on nanosized molybdenum clusters and quantum-cutting perovskite nanocrystals†

Jun Choi and Sung-Jin Kim *

A luminescent solar concentrator (LSC) is a photovoltaic (PV) device that uses luminophores embedded in waveguides to absorb and concentrate emitted solar energy to produce electricity. The most crucial factors enhancing the power conversion efficiency (PCE) of the LSC are high photoluminescence quantum yield (PLQY), low reabsorption, and low scattering of luminophores in a waveguide. We used a highly emissive molybdenum cluster anion, $[Mo_6I_8(CF_3COO)_6]^{2-}$, as a luminophore with a large Stokes shift to reduce reabsorption and scattering loss, and used quantum-cutting perovskite, Yb^{3+}-doped $CsPbCl_3$ nanocrystals, as a secondary luminophore with a high PLQY well over 100%. This dual-dye embedded LSC waveguide exhibited strong absorption in the ultraviolet region up to ~450 nm and emissions at 670 nm and 980 nm. The emission wavelengths of luminophore matched well with that of the external quantum efficiency (EQE) wavelength range of Si PV cell attached to the edge of the LSC waveguide, and its transparency could be utilized as highly efficient building-integrated photovoltaics (BIPV). LSCs with a PCE of 1.96% and an average visible transparency (AVT) of 68% and with a PCE of 1.62% and an AVT of 80% were fabricated. Our highly efficient and transparent LSCs are chemically stable and robust enough to be used as promising photovoltaic windows to realize zero-energy buildings.

Received 14th April 2024,
Accepted 21st June 2024

DOI: 10.1039/d4tc01520g

rsc.li/materials-c

Introduction

Luminescent solar concentrators (LSCs) are a promising solar energy–electric power conversion system. Typically, LSCs consist of polymeric matrices with embedded luminophores. LSCs capture incident solar light on their large front surface and redirect emissions of luminophores onto smaller photovoltaic (PV) cells on their edges, where photoluminescent photons are converted into electric current. LSCs have been a research topic since the 1970s because of their various advantages, such as aesthetic compatibility, transparency, and structural flexibility.[1] Among the various solar energy harvesting technologies, the LSCs have re-emerged and attracted significant attention as complementary devices to conventional Si PV solar panels.[2–6]

In the early days of LSC research, organic dyes were used as luminophores.[7,8] However, LSCs using these organic dyes as luminophores have disadvantages such as colors that are not suitable for windows, strong reabsorption due to large overlap between absorption and emission spectra, and limited stability under ultraviolet light. Our research focus is finding new chromophores for LSC window applications with high transparency and high power conversion efficiency. LSCs for architectural applications other than windows such as opaque walls and colorful roofs could be obtained using inorganic nanocrystals with better PLQYs. Lately, research activities have been focused on using inorganic nanocrystals such as core/shell quantum dots, metal clusters, and carbon dots.[9–26] However, to retain the emission efficiency and transparencies of inorganic nanocrystals, protection of their surface and uniform encapsulation in polymer waveguides are challenges that need to be overcome.

Recently, several semiconducting inorganic nanocrystals with large effective Stokes shifts and a high photoluminescence quantum yield (PLQY) have been explored for LSC applications.[27–31] Doping Yb^{3+} into $CsPbCl_3$ perovskite nanocrystals resulted in a surprisingly high PLQY approaching the limit of 200% *via* a quantum-cutting effect, and a significantly large Stokes shift was observed. Luo *et al.* reported a PLQY of 164% *via* a quantum-cutting effect in Yb^{3+}-doped $CsPbCl_3$.[27] Cai *et al.* synthesized Mn^{2+}/Yb^{3+}-codoped $CsPbCl_3$ nanocrystals and reported the highest total PLQY of 125.3% with triple-wavelength emissions

Department of Chemistry and Nano Science, Ewha Womans University, Seoul, 03760, Korea. E-mail: sjkim@ewha.ac.kr

† Electronic supplementary information (ESI) available. See DOI: https://doi.org/10.1039/d4tc01520g

covering UV, visible, and near-infrared regions due to the quantum-cutting effect.[28] The quantum-cutting effect in perovskite nanocrystals may offer a new opportunity to advance the LSC system with a higher power conversion efficiency (PCE) than that of undoped perovskite crystals.[32] However, there are few previous reports concerning the PCE of LSCs based on doped perovskite nanocrystals. Furthermore, no previous reports have demonstrated the credibility of LSC performance by confirming the consistency of photocurrents based on power PCE and external quantum efficiency (EQE) measurements. Importantly, PCE and average visible transparency (AVT) are often inversely related. Therefore, both parameters in LSCs should be considered for their potential in solar energy-harvesting window applications.

Previously, we reported an LSC with a PCE of 1.24% with ~85% transparency, where an inorganic–organic complex $(dMDAEMA)_4[Re_6S_8(NCS)_6]$ (dMDAEMA = 2-dimethyl amino ethyl(methacrylate)) and Zn-doped CuGaS/ZnS core/shell quantum dots were uniformly encapsulated in an amphiphilic polymer matrix.[33] This two-metal chalcogenide dye-embedded transparent LSC extended the harvesting coverage of the solar spectrum and reduced reabsorption and scattering. Energy transfer from ZnCuGaS/ZnS quantum dots to $(dMDAEMA)_4[Re_6S_8(NCS)_6]$ resulted in an enhanced PLQY of 33%, which was 1.7 times that of $(dMDAEMA)_4[Re_6S_8(NCS)_6]$. The emissions at 491 nm and 670 nm efficiently covered the EQE range of Si PV cells, resulting in an unprecedented combination of high PCE and transparency.

Here, we present a new combination of two optically complementary luminophores: the hexamolybdenum halide cluster organic–inorganic hybrid salt $(dMDAEMA)_2[Mo_6I_8(CF_3COO)_6]$ (MoC) and Yb^{3+}-doped $CsPbCl_3$, serving as quantum-cutting perovskite (QCP) nanocrystals. This pairing introduces a new avenue for LSCs in solar energy harvesting technologies. LSCs integrated with MoC and QCP absorb in the UV-A region of the solar spectrum and emit photoluminescence covering a larger fraction of the solar spectrum in the visible and IR regions, which are well-suited to Si PV cell-equipped LSCs. To validate our experimental findings, we conducted rigorous assessments of LSC photocurrent densities through EQE and PCE measurements, and we discuss the performance, transparency, and stability of LSCs underscoring their potential for building-integrated PVs.

Experimental section

Materials

To synthesize the hexamolybdenum cluster and quantum-cutting perovskites, lead acetate trihydrate ($Pb(OAc)_2{\cdot}3H_2O$, 99.9%), ytterbium acetate hydrate ($Yb(OAc)_3{\cdot}xH_2O$, 99.0%), cesium acetate (CsOAc, 99.9%), and chlorotrimethylsilane (TMS-Cl, 98%) were purchased from Alfa Aesar. 2-(Dimethylamino)ethyl methacrylate, 1-iodododecane, molybdenum (Mo, 99.9%), iodine (I_2, 99.8%), cesium iodide (CsI, 99.9%), silver trifluoroacetate (CF_3COOAg, 99.99%), oleylamine (OAm, 70%), 1-octadecene (ODE, 90%), oleic acid (OA, 90%), anhydrous ethanol, hexane, methyl methacrylate (MMA), and azobisisobutyronitrile (AIBN) were purchased from Sigma Aldrich. All chemicals were used as received without any purification.

Synthetic procedures

We prepared a salt consisting of an inorganic molybdenum cluster dianion with polymerizable organic cations forming $(dMDAEMA)_2[Mo_6I_8(CF_3COO)_6]$ (MoC). For the polymerizable cation $(dMDAEMA)^+$, 5 mL of 2-dimethylaminoethyl methacrylate (dMDAEMA) and 6.5 mL of 1-iodododecane were dissolved in 50 mL of chloroform and heated to 50 °C for 18 h. After heating, the reaction solution was concentrated using a rotary evaporator, and the product was precipitated with cold diethyl ether. After centrifugation, the filtered precipitates (dMDAEMA)I were washed repeatedly with cold diethyl ether and dried under vacuum.[34] $Cs_2[Mo_6I_8(CF_3COO)_6]$ used as a starting material of a luminophore was synthesized by substituting CF_3COO^- ligands for six I^- ligands in $Cs_2Mo_6I_{14}$.[35] Then, $Cs_2Mo_6I_{14}$ was synthesized from stoichiometric amounts of MoI_2 and CsI according to a procedure described in the literature.[36] The mixture of MoI_2 and CsI powder was formed into a pellet and placed in a vacuum-sealed silica tube, which was then heated for 72 hours at 700 °C. After the reaction, the product was confirmed by powder X-ray diffraction (XRD). To synthesize $Cs_2[Mo_6I_8(CF_3COO)_6]$, $Cs_2Mo_6I_{14}$ (2.21 mmol) and silver trifluoroacetate (CF_3COOAg) (13.26 mmol) were stirred in acetone (150 mL) for 24 h. The reaction was performed in the dark under an Ar atmosphere. After the ligand exchange reaction, the precipitated AgI was filtered, and the product solution was dried under vacuum to obtain an orange-colored powder of $Cs_2[Mo_6I_8(CF_3COO)_6]$. To synthesize $(dMDAEMA)_2[Mo_6I_8(CF_3COO)_6]$, 1.0 g of $Cs_2Mo_6I_{14}$ and 1.0 g (2.21 mmol) of dMDAEMAI were stirred in acetone (150 mL) for 24 h. The obtained product was filtered, and the solvent was evaporated using a rotary evaporator. The solid product was washed to remove excess CsI with a 1 : 1 mixture of CH_3OH and H_2O, yielding an orange-colored powder. To enhance the performance of LSCs by extending the solar light harvesting region with a high PLQY, Yb^{3+}-doped $CsPbCl_3$ (QCP) was prepared. For QCP synthesis, 5 mL of ODE, 0.5 mL of OAm, 1.0 mL of OA, 0.2 mmol of $Pb(OAc)_2{\cdot}3H_2O$, 280 μL of 1 M CsOAc in ethanol, and 0.16 mmol of $Yb(OAc)_3{\cdot}xH_2O$ were added to a 100 mL three-necked, round-bottom flask. The mixture was stirred and degassed for 5 min before heating to 110 °C for 1 h and then to 240 °C under Ar. Upon reaching 240 °C, 0.2 mL of TMS-Cl and 0.5 mL of ODE were injected into the flask. Immediately after injection, the flask was cooled to room temperature. The reaction solution was centrifuged at 3000 rpm for 15 min, and the product was washed with ethyl acetate.[28]

Fabrication of LSCs

To fabricate LSC waveguides, solutions of $(dMDAEMA)_2[Mo_6I_8(CF_3COO)_6]$ (MoC) in MMA at concentrations of 0.1, 0.2, 0.4, 0.8, and 1.0 wt% were sonicated for 30 minutes, and AIBN as an initiator for polymerization was added in a volume ratio of AIBN (μL) : MMA (mL) of 6 : 1. MoC–QCP LSCs were fabricated with mixtures of MoC : QCP wt% at ratios of 0.2 : 0.04, 0.2 : 0.1, 0.2 : 0.2, 0.2 : 0.45, and 0.2 : 0.6. These mixtures were sonicated

for 1 h to obtain homogeneous solutions. After sonication, each solution was poured into a glass mold and kept for drying in an oven for 24 h at 60 °C. The solution mixture was cooled into a hard polymer plate that was cut into the desired size and polished with sandpaper and cloth.

Characterization

Absorption spectra were recorded in the range of 280–800 nm using an Agilent Technologies G1103A UV/Vis spectrophotometer. The absorption and transmittance spectra of solid waveguides were recorded in a range of 280–800 nm with a Cary 5000 at 298 K. Emission spectra of luminophore solutions were obtained in the range of 450–1200 nm with a PerkinElmer LS 55 fluorescence spectrometer equipped with a xenon lamp at 298 K. The acetone solutions of MoC and QCP were de-aerated by bubbling with Ar gas prior to measurements. A quartz cell (Hellma, beam path length = 1.0 cm) was employed for solution samples. Photoluminescence spectra and the PLQY of solid LSC waveguide samples were recorded in the range of 450–1200 nm using a Horiba Fluorolog3 spectrophotofluorometer at an excitation wavelength of 375 nm at 298 K. The PLQY was determined using an integrating sphere coupled with a spectrofluorometer. This setup allowed us to accurately capture the emitted light and calculate the quantum yield by comparing the emitted light to the absorbed light. TEM measurement of QCP nanoparticles was performed using HRTEM (using a JEM-2100F) at the National Research Facilities and Equipment Center (NanoBioEnergy Materials Center) supported by the Korea Basic Science Institute (National Research Facilities and Equipment Center) at Ewha Womans University.

The PCE and EQE of LSCs were measured by illumination under a solar simulator at AM 1.5G (1000 mW cm^{-2}) (XES-201, SAN-EL ELECTRIC). For PCE measurements, 4 silicon PV cells were attached at the edges of the LSC and connected in parallel. The circumference of the front face of the LSC near the edges was masked with black electrical tape to avoid direct illumination of the solar source and to ensure the actual current was generated only from emission of luminophores in the LSC. For EQE measurements, one silicon PV cell was attached at the edge of the LSC waveguide, and the other 3 edges were masked with black electrical tape. The EQE of the Si PV cell was obtained in a range of 300–1100 nm using a solar cell IPCE measurement system (K3100 EQX, McScience). The current of the LSC system as a function of irradiation at various wavelengths was measured under a solar simulator using a home-built setup consisting of 23 bandpass interference filters. The EQE was measured by illuminating the LSC using a calibrated light source and recording the photocurrent generated by the silicon photovoltaic (PV) cells. This setup followed established protocols to ensure accurate and reproducible results. All measurements were performed at a standard temperature of 25 °C.

Results and discussion

We fabricated LSCs employing two dyes with broad emitting ranges in the red and NIR regions. Fig. 1a shows absorption and photoluminescence (PL) spectra of the two dyes dissolved in argon-saturated acetone solution. Also, the AM 1.5G solar spectrum and an EQE curve of the Si PV cell used for LSCs are shown. We selected a molybdenum cluster complex with a PLQY of approximately 29% as a phosphorescent luminophore. Molybdenum cluster complexes containing cluster anions $[\{Mo_6X_8\}Y_6]^{2-}$ (where X is an inner inorganic face-capping ligand and Y is an apical organic or inorganic ligand covalently bonded to the octahedral Mo_6 cluster) are well known inorganic emitters in the red and NIR regions.[36] Typically, molybdenum clusters emit broad red light between 600 and 800 nm and have a long luminescence lifetime of several microseconds. In order to produce highly transparent LSCs without aggregation of inorganic nanoclusters in the polymer waveguide, we prepared an organic–inorganic salt (MoC) consisting of a nanosized inorganic cluster anion $[Mo_6I_8(CF_3COO)_6]^{2-}$ and polymerizable organic cation $(dMDAEMA)^+$ to generate $(dMDAEMA)_2[Mo_6I_8(CF_3COO)_6]$. $(dMDAEMA)^+$ cations in MOC were copolymerized with an organic solvent, methyl methacrylate (MMA), to form an amphiphilic MoC-PMMA hybrid. The organic cation $dMDAEMA^+$ has a long aliphatic chain ($C_{12}H_{15}$) at one end that allows high solubility in MMA. The other end of the cation has a methacrylate functional group, which is suitable for copolymerization with MMA. To extend the coverage of the energy harvest range of the Si PV cell, we used Yb^{3+}-doped $CsPbCl_3$ perovskite (QCP) nanocrystals as a secondary luminophore that emits PL in the NIR region of 900–1100 nm. Generally, dyes that emit light in the NIR region have the disadvantage of a low PLQY; however, QCP overcomes this disadvantage through a quantum-cutting effect. Quantum-cutting luminophores can absorb single high-energy photons and emit two lower-energy photons, approaching the theoretical PLQY limit of 200%. When two dyes were added to the LSC fabrication process to form the MoC-QCP–PMMA hybrid, nanosized anionic $[Mo_6I_8(CF_3COO)_6]^{2-}$ metal clusters and $Pb_{1-x}Yb_xCl_3{}^{\delta-}$ nanoparticles were immobilized uniformly on cationic sites of the PMMA matrix (Fig. 1b). Fig. 2a shows a schematic illustration of the crystal structure of QCP forming $Cs_{1-x}Pb_{1-x}Yb_xCl_3$. The powder X-ray diffraction (XRD) pattern of QCP indicated a typical cubic perovskite phase. However, the diffraction peaks were shifted slightly to higher diffraction angles than those of the undoped $CsPbCl_3$ phase, indicating a decrease in lattice parameters (Fig. S1, ESI†). This effect is due to substitution of Pb^{2+} ions of 132 pm by the smaller Yb^{3+} of 100 pm in $Cs_{1-x}Pb_{1-x}Yb_xCl_3$. $CsPbCl_3$ dissolved in hexane exhibited emission with a maximum peak at 403 nm (Fig. S2, ESI†). However, the QCP solution exhibited an intense emission peak in the near-infrared region at ~980 nm as shown in Fig. 1a, which originated from the quantum-cutting effect due to effective excitation energy transfer from the $CsPbCl_3$ host to doped Yb^{3+}. In QCP, a single high-energy photon at 403 nm splits into two low-energy photons in the near-infrared region at ~980 nm by the quantum-cutting effect, as illustrated in Fig. 2b. It is known that QCP absorbs a single photon to obtain the excited state, which down-converts into low-energy photons, corresponding to Yb^{3+} $2F_{5/2} \rightarrow 2F_{7/2}$ emission and resulting in a favorable PLQY as high as 193%.[37] The QCP crystals had a

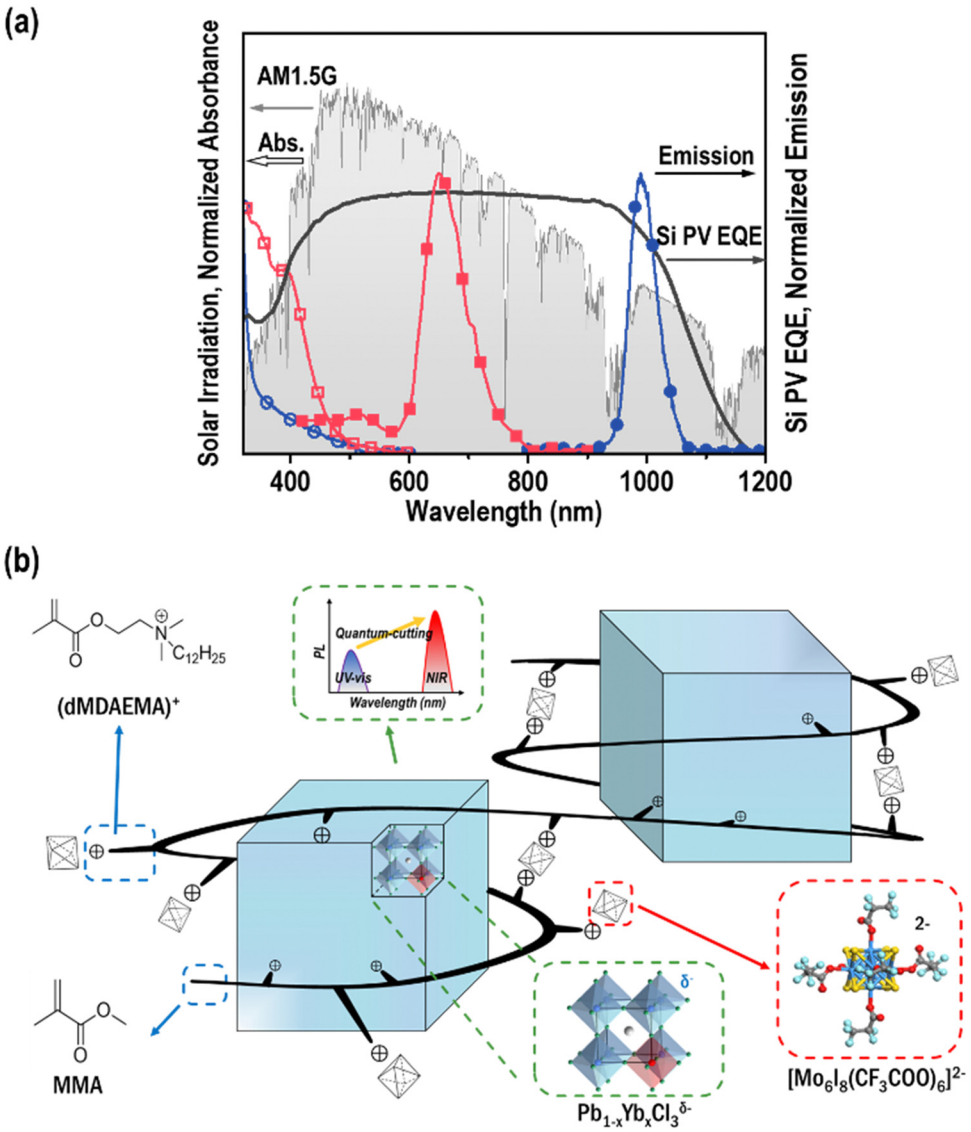

Fig. 1 (a) Normalized absorption (open symbol) and PL (solid symbol) spectra of MoC (red squares) and QCP (blue circles) dissolved in argon-saturated acetone solution. The AM 1.5G solar spectrum (gray shading) and an EQE curve of the Si PV cell (black solid line) used for LSCs. (b) Illustration of the metal cluster- and QCP-embedded polymer hybrid MoC + QCP-PMMA. The polymerizable organic cation dMDAEMA^{+} is copolymerized with MMA monomers such that the metal cluster anions and $Pb_{1-x}Yb_xCl_3^{\delta-}$ nanocrystal surfaces are immobilized on cation sites of the polymer chain backbone, isolating each cluster in the PMMA matrix. Also, the negative surface of perovskites was immobilized between cationic polymers.

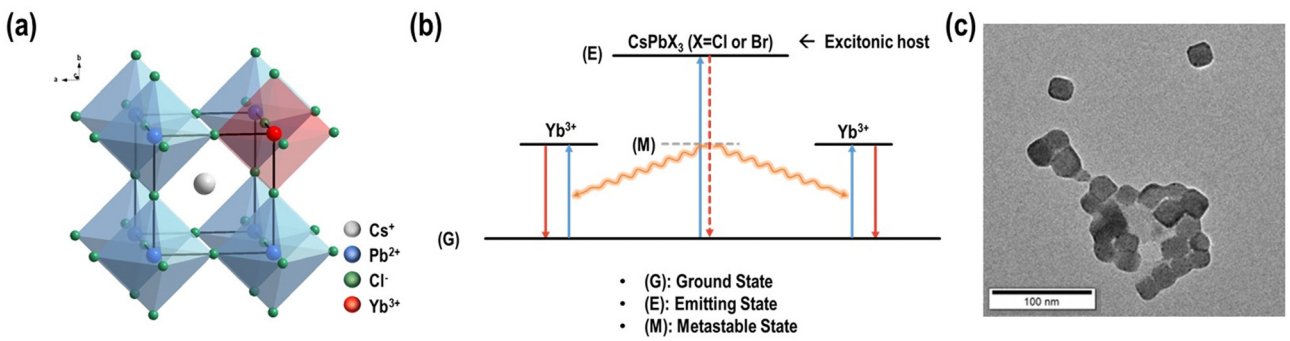

Fig. 2 (a) Schematic illustration of the QCP crystal structure. (b) Schematic of the quantum-cutting process of Yb^{3+}-doped $CsPbCl_3$ perovskite nanocrystals. Absorption of a single high-energy photon (blue) and emission of two lower-energy photons (red). (c) TEM image of QCP.

uniform cubic shape with an average size of 8 ± 0.7 nm as shown in the transmission electron microscopy (TEM) image of Fig. 2c.

To optimize LSCs in terms of PCE and transparency, dual-dye-embedded waveguides with various concentrations of MoC and QCP were fabricated by adding 0.04, 0.1, 0.2, 0.45, and 0.6 wt% QCP to 0.2 wt% MoC in MMA solution (hereafter we denote dual dyes as MoC + QCP and concentration ratios of MoC and QCP in wt% as 0.2 : 0.04, 0.2 : 0.1, 0.2 : 0.2, 0.2 : 0.45, 0.2 : 0.6). For comparison, single luminophore-encapsulated LSCs were fabricated with various concentrations of MoC. To assess the transparency of a device, average visible transmittance (AVT) and color rendering index (CRI) were measured. For architectural purposes suitable for building-integrated photovoltaic windows, the LSC waveguides require an AVT of 70–90%.[38,39] Transmittance in the visible wavelength range of 380–780 nm varied depending on the concentration of dyes as shown in Fig. 3a. The 0.2 wt%-MoC-embedded LSC without QCP showed a high AVT of 84.9%. The transmittance gradually decreased as the quantity of QCP was increased. The dual-dye-embedded LSC with MoC + QCP (0.2 : 0.1 wt%) was clear, with an AVT of 80%; however, LSCs with MoC + QCP (0.2 : 0.6 wt%) became hazy, with an AVT of 68%. A photograph of a large-sized LSC with MoC + QCP (0.2 : 0.1 wt%) in daylight exhibited high transmittance without haziness as shown in Fig. 3b, which indicates uniform distribution of nano-sized dyes without aggregation due to the electrostatic interactions between nano-sized anionic $[Mo_6I_8(CF_3COO)_6]^{2-}$ clusters and $Pb_{1-x}Yb_xCl_3^{\delta-}$ of QCP nanoparticles with cationic sites of the PMMA matrix. The color coordinates of the LSCs also showed nearly neutral color detection. As the concentration of the QCP was increased, the color coordinates deviated only slightly from the center of the color plane (0.3, 0.3). Detailed AVTs and color coordinates for different samples with different dye concentrations are summarized in Table S1 (ESI†).

We measured the PLQYs of the dyes embedded in the LSC plate, and the results are shown in Table S2 (ESI†). The absolute PLQYs of $Cs_2Mo_6I_{14}$ and MoC in the LSC polymer matrix were

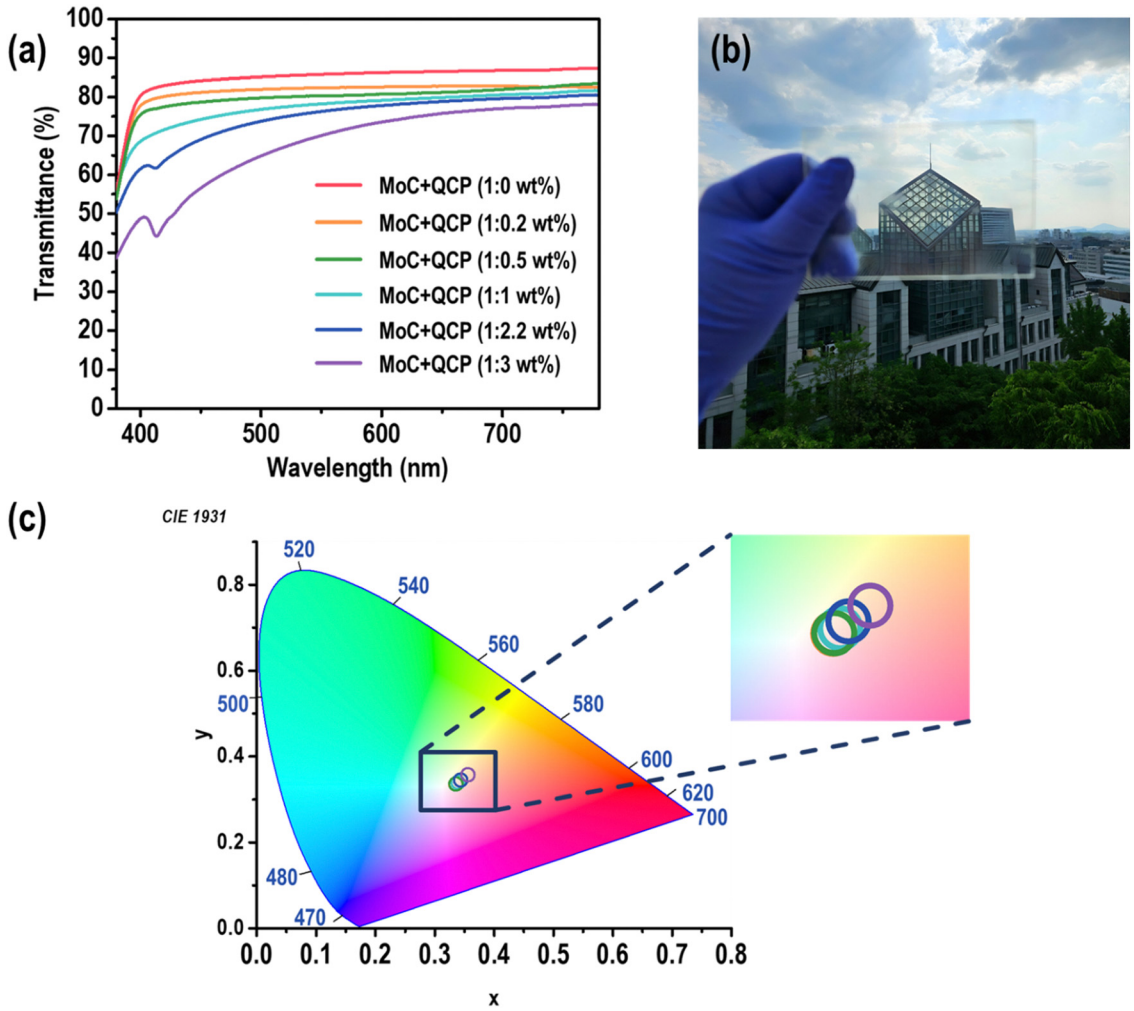

Fig. 3 (a) Transmittance spectra of LSCs with various concentrations of MoC and QCP. (b) Photograph of a large LSC (MoC + QCP 0.2 : 0.1 wt%). (c) A CIE 1931 color space chromaticity diagram reporting the color coordinates of LSCs with various dye concentrations. The color coordinates (*x* and *y*) for each sample are listed in Table S1 (ESI†).

1% and 31%, respectively. Therefore, the choice of inorganic ligands of a metal cluster and organic cations can significantly improve the cluster's PLQY. The CF_3COO^- ligands in MoC attract more electrons from $[Mo_6I_8]^{4+}$ than do I^- ligands in $Cs_2Mo_6I_{14}$, which results in more stable excited states and fewer non-radiative decay states. $CsPbCl_3$ emitted PL with a maximum peak at 403 nm, and its PLQY was approximately 8.3%. However, the QCP exhibited emission in the NIR region of 900–1200 nm with a PLQY of 109.9% due to the quantum-cutting effect from Yb^{3+} doping. The solid LSC waveguide embedded with MoC and QCP in a ratio of 0.2 : 0.1 wt% exhibited a PLQY of 92.4%, which is mainly due to the strong PL of QCP at ~980 nm. The PL spectrum of the dual-dye LSC (MoC + QCP with a ratio of 0.2 : 0.1 wt%) is shown in Fig. S3 (ESI†). The PLQY measurements were performed using an excitation wavelength of 375 nm on the MoC- and QCP-embedded solid LSC waveguide with a size of $10 \times 10 \times 3$ mm^3.

The performance of LSCs can be evaluated by the PCE, which is defined as the ratio of electrical power output to incident power. The PCE can be calculated as PCE = $(J_{SC} \times V_{OC} \times FF)/P_{in}$, where J_{SC} is the short-circuit density, V_{OC} is the open-circuit voltage, FF is the fill factor, and P_{in} is the incident power. For PCE measurements, LSCs were fabricated with various concentrations of MoC and QCP with dimensions of $25 \times 25 \times 3$ mm^3. The LSCs were equipped with four Si PV cells (25×3 mm^2) on the edges of the waveguide, and the perimeter of the front face was masked with black tape to prevent direct sunlight on Si PV cells except in an actual light harvesting area of 20×20 mm^2. The Si PV cell used for PCE measurement has an efficiency of about 14.0%, and the PCE and EQE of the Si PV cell are shown in Fig. S4 and S5 (ESI†). The four Si PV cells were connected in parallel. The LSC *J–V* curves and PV parameters including J_{SC}, V_{OC}, and FF are extracted from Fig. 4b, and the results are summarized in Table 1. For the LSC with MoC 0.2 wt%, the highest PCE was 1.40% with a J_{SC} of 5.16 mA cm^{-2}. For the LSC with QCP 0.1 wt%, the highest PCE was 1.40% with a J_{SC} of 5.47 ± 0.05 mA cm^{-2}. The higher PCE of the QCP-embedded LSC compared to a PCE of 0.96% for the undoped-$CsPbCl_3$ can be attributed to the increase in the PLQY of the luminophore by Yb^{3+} doping. In LSCs with a concentration ratio of MoC : QCP (0.2 : 0.6 wt%), a PCE of 1.91 ± 0.02% was observed.

The efficiency of the LSC can be presented in terms of the optical efficiency, $\eta_{OPT} = \int (1 - R(\lambda))\left(1 - e^{\alpha_C(\lambda)d}\right)\left(1 - e^{\alpha_{wg}(\lambda)L}\right)\eta_{trap}\phi_{PL}(1 - \eta_S(\lambda))(1 - \eta_{RA}(\lambda))d\lambda$. η_{OPT} is based on the working principle of LSC in Fig. 4a, where $R(\lambda)$ is the waveguide front-face reflection, and $e^{\alpha C(\lambda)}$ and $e^{\alpha wg(\lambda)}$are the absorption coefficients of the luminophore and matrix, respectively. d and L are the thickness and length of the LSC, respectively. η_{trap} is the trapping efficiency, which represents how effectively the LSC captures incident sunlight and confines it within the waveguide. When PMMA with a refractive index of 1.5 is used as the matrix for LSC, the calculated maximum η_{trap} is approximately 75%. ϕ_{PL} is the PL quantum yield of the luminophore, $\eta_S(\lambda)$ is the scattering suppression efficiency due to optical imperfection of the waveguide, and $\eta_{RA}(\lambda)$ is the reabsorption suppression efficiency due to multiple reabsorptions and re-emissions within the waveguide.[2] To increase the LSC efficiency, it is crucial to select luminophores with high PLQY, low scattering, and low reabsorption loss. Recent studies have introduced the concept of external optical efficiency (η_{ext}), which serves as a comprehensive measure accounting for all losses and energetic phenomena in the LSC system, providing a viable substitute for the conventional η_{OPT}. The η_{ext} of the LSC can be expressed as $\eta_{ext} = \eta_{abs} \times \eta_{int}$, where η_{int} is the internal optical efficiency; the ratio between edge-emitted photons and incident solar photons are related, with $\eta_{int} = \eta_{trap} \times \phi_{PL}$.[27] We evaluated η_{ext} from measurement of η_{int} and η_{abs} to compare the values with previous reports of perovskite luminophores and the values of dual-dye LSCs were evaluated. The η_{abs} of $CsPbCl_3$ and QCP in the solid state were similar at 3.1% and 3.3%, respectively, indicating similar electronic structures of the two phases. The measurements performed for dual-dye LSCs using an integrating sphere yielded η_{trap} of 74 ± 0.2% for the optimized dual-dye concentration of MoC : QCP (0.2 : 0.6 wt%). The η_{ext} values of $CsPbCl_3$ and QCP were calculated to be 0.19% and 2.7%, respectively, which are mainly due to significant changes from ϕ_{PL} = 8.3% to 110.8% by the quantum-cutting effect of QCP.[30,40] In our dual-dye-embedded LSC with MoC and QCP in ratios of 0.2 : 0.1 wt%, the external optical efficiency was η_{ext} = 4.2%, which is much higher than the 2.7% for the perovskite-based single-dye-embedded LSC. LSCs with a ratio of MoC : QCP = 0.2 : 0.6 wt% showed a higher η_{ext} = 4.9%. The LSC with MoC : QCP = 0.2 : 0.6 wt% and MoC : QCP = 0.2 : 0.1 wt% exhibited PCE of 1.91% with an AVT of ~68% and PCE of 1.62% with a transparency of 80%, respectively. Summary of dye concentrations, photovoltaic parameters measured from PCE measurements, external optical efficiency η_{ext}, and average visible transmission are shown in Table 1. The results indicated that the PCE of dual-dye LSCs could be improved by 16–40% by adding 0.1–0.6 wt% QCP to MoC, without a significant reduction of transparency. However, QCP concentrations higher than 0.6 wt% resulted in an unsatisfactory low transparency for window applications.

Optical efficiencies η_{ext} ~10% higher than that of our QCP LSC in further modified Yb^{3+}-doped perovskite, such as $CsPbCl_xBr_{3-x}$ LSC have been reported by Luo *et al.*[20] Chen *et al.* synthesized Mn^{2+}/Yb^{3+}-codoped $CsPbCl_3$ nanocrystals and reported a 14-fold higher PLQY of 125.3% due to triple-wavelength emission covering UV, visible, and near-infrared regions with an η_{ext} of 9.6%.[28] In the case of a one dye system such as perovskite, a higher η_{ext} may suggest a higher PCE of the LSC. Since the η_{ext} values represent the intrinsic optical properties of the dyes, they are not directly correlated with the efficiency of LSCs. To assess the efficiency of LSCs accurately, it is essential to measure the PCE, which reflects the influence of scattering and reabsorption phenomena within the waveguide, as well as the impact of Si PV cells. Furthermore, there is a trade-off between PCE and transparency, and the two factors should be optimized for realization of LSCs for potential building-integrated PV application. However, there is a scarcity of previous reports concerning both PCE and transparency of LSCs based on doped perovskite nanocrystals. Our results on two-dye LSCs suggested that achieving a high PCE without the typical trade-off in transparency was feasible.

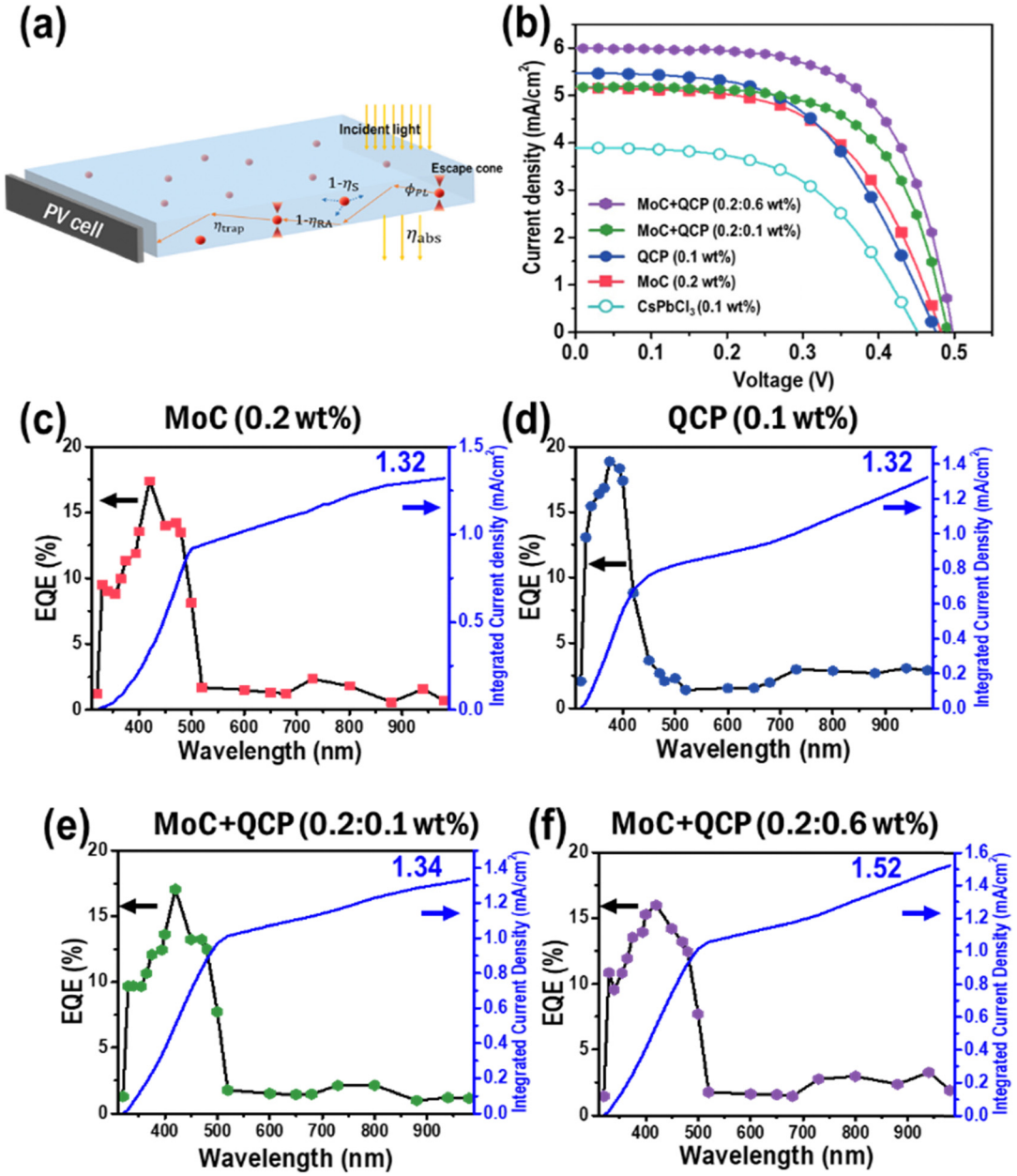

Fig. 4 (a) Schematic representation of the LSC working principle. (b) Current density–voltage (*J*–*V*) curves of LSCs with various concentrations of MoC and QCP. The EQE spectrum of an LSC system with a size of 25 × 25 × 3 mm^3 for dyes of (c) MoC (0.2 wt%) (red squares), (d) QCP (0.1 wt%) (blue circles), (e) MoC + QCP (0.2 : 0.1 wt%) (green hexagons), and (f) MoC + QCP (0.2 : 0.6 wt%) (purple hexagons), and the blue line is the current density obtained by integrating each spectrum.

Table 1 Summary of dye concentration, photovoltaic parameters measured from power conversion efficiency (PCE) measurements, external optical efficiency η_{ext}, and average visible transmission. The PCE was measured from the LSC with a front surface area of 20 mm × 20 mm × 3 mm

Dyes (wt% in MMA solution for LSC waveguide)	J_{SC} (mA cm^{-2})	V_{OC} (V)	FF	PCE (%)	η_{ext} (%)	AVT
$CsPbCl_3$ (0.1)	3.90	0.451	0.543	0.96	0.19	—
QCP (0.1)	5.47	0.476	0.539	1.40	2.7	80.4
MoC (0.2)	5.16	0.482	0.563	1.40	1.3	84.9
MoC + QCP (0.2 : 0.1)	5.18	0.491	0.636	1.62	4.2	80.0
MoC + QCP (0.2 : 0.6)	5.99	0.498	0.640	1.91	4.9	67.9

We carried out EQE measurements to examine the validity of PCE by comparing the consistency of J_{SC}s with that of the extracted value from PCE measurements. The EQE measurements were performed with one Si PV cell attached to an edge of the LSC with a home-built set-up consisting of a 1000 W xenon lamp light source and 23 bandpass interference filters covering the 320–980 nm region. The EQE (λ) of the device was calculated as

$$\mathrm{EQE}(\lambda) = \mathrm{EQE}^{\mathrm{ref}}(\lambda) \times \frac{I_{\mathrm{LSC}}}{I_{\mathrm{PV}}^{\mathrm{ref}}} \quad (1)$$

where $EQE^{ref}(\lambda)$ and I_{ref}^{PV} are the EQE and short-circuit current of the PV cell as a function of wavelength, respectively. The short-circuit current of the LSC is expressed as I_{ISC} and was measured under a solar simulator as a function of wavelength with bandpass filters. For the LSC with only MoC, the J_{SC} obtained by integrating the EQE spectra was 1.32 mA cm^{-2}, which shows a good agreement of 98% compared to 1.29 mA cm^{-2}, which is one-fourth of 5.16 mA cm^{-2} obtained through the PCE measurement from four edges of the LSC. In the LSC with only QCP, the integrated current density was 1.32 mA cm^{-2}, showing a good match of 97% compared with the current density of 1.37 mA cm^{-2} obtained through PCE measurement. LSCs with MoC and QCP as dual dyes also showed good agreements of 97% and 98%, respectively, with 1.34 mA cm^{-2} for MoC + QCP (0.2 : 0.1 wt%)-LSC and 1.52 mA cm^{-2} for MoC + QCP (0.2 : 0.6 wt%)-LSC. The QCP-rich LSC with MoC + QCP (0.2 : 0.6 wt%) showed a relatively high EQE in the 700–980 nm region due to high scattering among particles. In the EQE measurement, the current density value obtained from one PV cell multiplied by 4 is equivalent to the value measured using four PV cells, ensuring that our single-cell setup accurately reflects the performance of the LSC-PV system. This equivalency has been validated and aligns with established protocols as described in the literature.[41]

To investigate the reabsorption loss within the LSC waveguide, we measured the Si PV response as a function of the distance (d) between the PV cell and the center of the excitation site.[13,42–45] As shown in Fig. 5a and b, an 80 × 100 × 3 mm^3 LSC with a PV cell attached on one edge was fabricated, and the 20 × 20 mm^2 area of the LSC face was irradiated. The distance d between the center of the excitation site and the PV cell was increased from 1 to 8 cm, and the current as Si PV responses was measured. It was anticipated that as d increased, J_{SC} would decrease due to the combined effects of reabsorption and scattering loss by the dyes, as well as photon escape loss from the waveguide. The J_{SC} with increasing d in the LSC incorporating only MoC exhibited ∼45% reduction for the 8 cm distance compared with the maximum J_{SC} achieved near the PV cell, which is a typical feature of PL flux decrease due to the photon escape loss. However, the LSC incorporating $CsPbCl_3$ nanocrystals exhibited severe reduction of J_{SC} > 90%, which is a similar feature to previously known inorganic quantum dot containing LSCs with an additional scattering loss to the photon escape loss. The LSC incorporating $CsPbCl_3$ showed a low J_{SC} of 3.76 mA cm^{-2} due to its low PLQY, which was greatly reduced to 0.32 mA cm^{-2} when d was increased to 8 cm, an indication of high levels of reabsorption and scattering loss. However, the J_{SC} reduction as a function of d was not significant in dual-dye LSCs compared to single-dye LSCs. When d was increased to 8 cm, current density reductions of 46.2% and 64.2% were observed for MoC + QCP (0.2 : 0.1) and MoC + QCP (0.2 : 0.6), respectively. The significant reduction observed in MoC + QCP (0.2 : 0.6 wt%) can be attributed to the less uniform distribution of the more abundant inorganic QCP nanocrystals within the polymer matrix. It is clear that while the higher concentration of QCP resulted in a higher current density near the PV cell, it also resulted in severe scattering loss at higher d. The J_{SC} reduction of 46.2% in MoC + QCP (0.2 : 0.1) is not much different from the ∼40% in the only-MoC-embedded LSC due to the typical photon escape effect from the waveguide. However, the current density reduction of 64.2% for MoC + QCP (0.2 : 0.6 wt%) is significantly smaller than the 80% reduction for QCP nanocrystals without MoC. Therefore, MoC in LSCs reduces scattering loss due to nanocrystals by anchoring them in the MoC-polymer hybrid matrix.

In further experiments, the stability of LSCs embedded with various luminophores was studied. The LSC plates were left in a normal laboratory environment, and the current density of the LSCs was measured every 30 days for 90 days. The LSC incorporating $CsPbCl_3$ maintained 80% of the current density after 90 days compared to 94% for MoC-, 88% for QCP-, 95% for MoC + QCP (0.2 : 0.1 wt%)-, and 92% for MoC + QCP (0.2 : 0.6 wt%)-containing LSCs. As shown in Fig. S6 (ESI†), all samples maintained a current density greater than 80% even after 90 days. This result demonstrated that the stability and low scattering loss due to uniform dispersion of nano-sized dyes by anchoring in modified PMMA provide additional advantages for LSC fabrication in the development of zero-energy PV buildings.

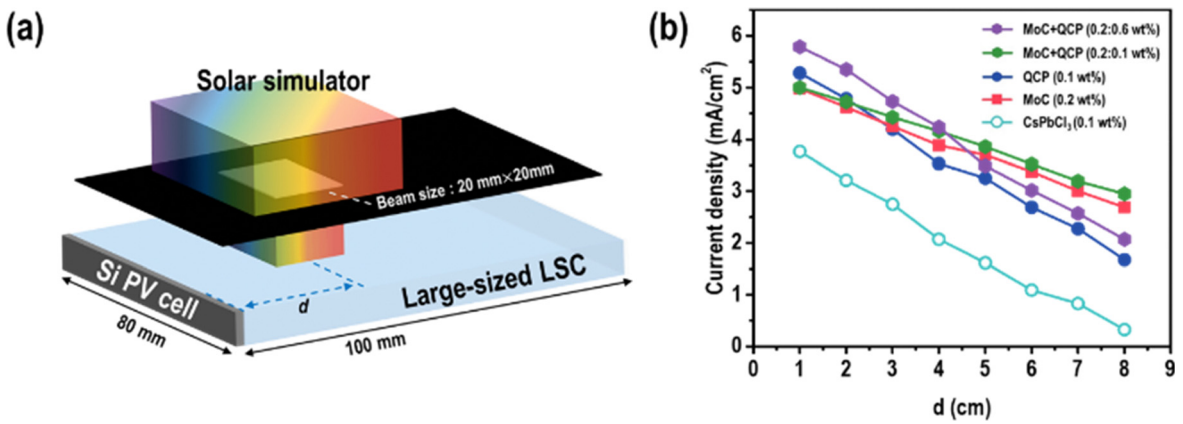

Fig. 5 (a) Schematic representation of the current density measurement of LSCs as a function of the distance between the center of the illumination area and the PV cell located at the edge of the LSC plates. (b) Current density as a function of distance (d) for various dye-incorporated LSCs.

Conclusions

We fabricated LSCs with inorganic–organic hybrid cluster (MoC) salt and inorganic quantum-cutting perovskite (QCP) nanocrystals as luminophores by encapsulating them within an amphiphilic polymer matrix. The PCE of LSCs embedded with MoC dye improved from 1.40% to 1.91% upon addition of the QCP dye. The improvement in PCE is attributed to the high PLQY of QCP, low reabsorption losses due to large Stokes shifts of the two dyes, and reduced scattering loss due to the uniform dispersion of the two dyes in an amphiphilically modified polymer matrix. The broad emission at 600–800 nm of MoC and the strong emission at 986 nm due to the quantum-cutting effect of the QCP extended solar light harvest coverage of Si PV cells resulting significantly improved PCE. We demonstrated new chemically and optically complementary dyes for an efficient and transparent LSC system which show promise as solar energy-harvesting windows for urban buildings.

Author contributions

J. C. and S. K. designed the experiments and wrote the manuscript. J. C. synthesized the materials, fabricate device, performed the UV-vis, PL, and EQE, *J–V* curve measurements, stabilized photocurrent densities and data analysis. J. C and S. K. wrote and revised the final manuscript. All the authors reviewed the manuscript.

Data availability

The data that support the findings of this study are available from the corresponding author upon reasonable request. This includes raw and processed data for the optical properties characterization, EQE measurements, and other experimental results discussed in the manuscript. Additionally, any ESI† files and datasets generated during and/or analyzed during the current study are included with this article.

Conflicts of interest

There are no conflicts to declare.

Acknowledgements

This work was supported by the National Research Foundation of Korea (NRF) grant funded by the Korean government (MSIT) (NRF-2021R1A2C2091348).

References

1 W. H. Weber and J. Lambe, Luminescent Greenhouse Collector for Solar Radiation, *Appl. Opt.*, 1976, **15**(10), 2299–2300.
2 R. Mazzaro and A. Vomiero, The Renaissance of Luminescent Solar Concentrators: The Role of Inorganic Nanomaterials, *Adv. Energy Mater.*, 2018, **8**(33), 1801903.
3 M. G. Debije and P. P. C. Verbunt, Thirty Years of Luminescent Solar Concentrator Research: Solar Energy for the Built Environment, *Adv. Energy Mater.*, 2012, **2**(1), 12–35.
4 W. G. J. H. M. Van Sark, Luminescent Solar Concentrators - A Low Cost Photovoltaics Alternative, *Renew Energy*, 2013, **49**, 207–210.
5 M. G. Debije, Solar Energy Collectors with Tunable Transmission, *Adv. Funct. Mater.*, 2010, **20**(9), 1498–1502.
6 F. Meinardi, F. Bruni and S. Brovelli, Luminescent Solar Concentrators for Building-Integrated Photovoltaics, *Nat. Rev. Mater.*, 2017, **2**(12), 17072.
7 L. H. Slooff, E. E. Bende, A. R. Burgers, T. Budel, M. Pravettoni, R. P. Kenny, E. D. Dunlop, A. Buchtemann and A. Luminescent Solar, Concentrator with 7.1% Power Conversion Efficiency, *Phys. Status Solidi RRL*, 2008, **2**(6), 257–259.
8 S. J. Ha, J. H. Kang, D. H. Choi, S. K. Nam, E. Reichmanis and J. H. Moon, Upconversion-Assisted Dual-Band Luminescent Solar Concentrator Coupled for High Power Conversion Efficiency Photovoltaic Systems, *ACS Photonics*, 2018, **5**(9), 3621–3627.
9 Y. F. Zhou, H. G. Zhao, D. L. Ma and F. Rosei, Harnessing the Properties of Colloidal Quantum Dots in Luminescent Solar Concentrators, *Chem. Soc. Rev.*, 2018, **47**(15), 5866–5890.
10 M. G. Hyldahl, S. T. Bailey and B. P. Wittmershaus, Photo-Stability and Performance of CdSe/ZnS Quantum Dots in Luminescent Solar Concentrators, *Sol. Energy*, 2009, **83**(4), 566–573.
11 I. Coropceanu and M. G. Bawendi, Core/Shell Quantum Dot Based Luminescent Solar Concentrators with Reduced Reabsorption and Enhanced Efficiency, *Nano Lett.*, 2014, **14**(7), 4097–4101.
12 C. S. Erickson, L. R. Bradshaw, S. McDowall, J. D. Gilbertson, D. R. Gamelin and D. L. Patrick, Zero-Reabsorption Doped-Nanocrystal Luminescent Solar Concentrators, *ACS Nano*, 2014, **8**(4), 3461–3467.
13 F. Meinardi, H. McDaniel, F. Carulli, A. Colombo, K. A. Velizhanin, N. S. Makarov, R. Simonutti, V. I. Klimov and S. Brovelli, Highly Efficient Large-Area Colourless Luminescent Solar Concentrators using Heavy-Metal-Free Colloidal Quantum Dots, *Nat. Nanotechnol.*, 2015, **10**(10), 878–885.
14 H. G. Zhao, D. Benetti, L. Jin, Y. F. Zhou, F. Rosei and A. Vomiero, Absorption Enhancement in "Giant" Core/Alloyed-Shell Quantum Dots for Luminescent Solar Concentrator, *Small*, 2016, **12**(38), 5354–5365.
15 R. Sumner, S. Eiselt, T. B. Kilburn, C. Erickson, B. Carlson, D. R. Gamelin, S. McDowall and D. L. Patrick, Analysis of Optical Losses in High-Efficiency $CuInS_2$-Based Nanocrystal Luminescent Solar Concentrators: Balancing Absorption versus Scattering, *J. Phys. Chem. C*, 2017, **121**(6), 3252–3260.
16 S. Sadeghi, H. B. Jalali, R. Melikov, B. G. Kumar, M. M. Aria, C. W. Ow-Yang and S. Nizamoglu, Stokes shift-Engineered Indium Phosphide Quantum Dots for Efficient Luminescent Solar Concentrators, *ACS Appl. Mater. Interfaces*, 2018, **10**(15), 12975–12982.

17 K. F. Wu, H. B. Li and V. I. Klimov, Tandem Luminescent Solar Concentrators Based on Engineered Quantum Dots, *Nat. Photonics*, 2018, **12**(2), 105–111.
18 S. K. E. Hill, R. Connell, C. Peterson, J. Hollinger, M. A. Hillmyer, U. Kortshagen and V. E. Ferry, Silicon Quantum Dot-Poly(methyl methacrylate) Nanocomposites with Reduced Light Scattering for Luminescent Solar Concentrators, *ACS Photonics*, 2019, **6**(1), 170–180.
19 J. Huang, J. J. Zhou, T. Haraldsson, A. Clemments, M. Fujii, H. Sugimoto, B. Xu and I. Sychugov, Triplex Glass Laminates with Silicon Quantum Dots for Luminescent Solar Concentrators, *Sol. RRL*, 2020, 2000195.
20 J. Chen, H. Zhao, Z. Li, X. Zhao and X. Gong, Highly efficient tandem luminescent solar concentrators based on eco-friendly copper iodide based hybrid nanoparticles and carbon dots, *Energy Environ. Sci.*, 2022, **15**(2), 799–805.
21 J. Lin, L. Wang, Q. Jing and H. Zhao, Highly efficient and high color rendering index multilayer luminescent solar concentrators based on colloidal carbon quantum dots, *J. Chem. Eng.*, 2024, **481**, 148441.
22 J. Li, H. Zhao, X. Zhao and X. Gong, Boosting efficiency of luminescent solar concentrators using ultra-bright carbon dots with large Stokes shift, *Nanoscale Horiz.*, 2023, **8**, 83–94.
23 J. Li, J. Chen, X. Zhao, A. Vomiero and X. Gong, High-loading of organosilane-grafted carbon dots in high-performance luminescent solar concentrators with ultra-high transparency, *Nano Energy*, 2023, **115**, 108674.
24 W. Li, X. Wang, J. Lin, X. Meng, L. Wang, M. Wang, Q. Jing, Y. Song, A. Vomiero and H. Zhao, Controllable and large-scale synthesis of carbon quantum dots for efficient solid-state optical devices, *Nano Energy*, 2024, **122**, 109289.
25 Y. You, X. Tong, A. Imran Channa, H. Zhi, M. Cai, H. Zhao, L. Xia, G. Liu, H. Zhao and Z. Wang, High-efficiency luminescent solar concentrators based on Composition-tunable Eco-friendly Core/shell quantum dots, *J. Chem. Eng.*, 2023, **452**, 139490.
26 K.-B. Cai, H.-Y. Huang, M.-L. Hsieh, P.-W. Chen, S.-E. Chiang, S. Hsiung Chang, J.-L. Shen, W.-R. Liu and C.-T. Yuan, Two-Dimensional Self-Assembly of Boric Acid-Functionalized Graphene Quantum Dots: Tunable and Superior Optical Properties for Efficient Eco-Friendly Luminescent Solar Concentrators, *ACS Nano*, 2022, **16**(3), 3994–4003.
27 X. Luo, T. Ding, X. Liu, Y. Liu and K. F. Wu, Quantum-Cutting Luminescent Solar Concentrators Using Ytterbium-Doped Perovskite Nanocrystals, *Nano Lett.*, 2019, **19**(1), 338–341.
28 T. Cai, J. Y. Wang, W. H. Li, K. Hills-Kimball, H. J. Yang, Y. Nagaoka, Y. C. Yuan, R. Zia and O. Chen, Mn^{2+}/Yb^{3+} Codoped CsPbCl3 Perovskite Nanocrystals with Triple-Wavelength Emission for Luminescent Solar Concentrators, *Adv. Sci.*, 2020, **7**(18), 2001317.
29 M. J. Crane, D. M. Kroupa and D. R. Gamelin, Detailed-Balance Analysis of Yb^{3+}:$CsPb(Cl_{1-x}Br_x)(3)$ Quantum-Cutting Layers for High-Efficiency Photovoltaics Under Real-World Conditions, *Energy Environ. Sci.*, 2019, **12**(8), 2486–2495.
30 T. A. Cohen, T. J. Milstein, D. M. Kroupa, J. D. MacKenzie, C. K. Luscombe and D. R. Gamelin, Quantum-Cutting Yb^{3+} - Doped Perovskite Nanocrystals for Monolithic Bilayer Luminescent Solar Concentrators, *J. Mater. Chem. A*, 2019, **7**(15), 9279–9288.
31 S. M. Ferro, M. Wobben and B. Ehrler, Rare-Earth Quantum Cutting in Metal Halide Perovskites - A Review, *Mater. Horiz.*, 2021, **8**(4), 1072–1083.
32 A. B. Stefania Castelletto, Luminescence Solar Concentrators: A Technology Update, *Nano Energy*, 2023, **109**, 108269–108286.
33 J. Choi, K. Kim and S.-J. Kim, Quantum Dot Assisted Luminescent Hexarhenium Cluster Dye for a Transparent Luminescent Solar Concentrator, *Sci. Rep.*, 2021, **11**, 13833.
34 O. A. Efremova, K. A. Brylev, Y. A. Vorotnikov, L. Vejsadova, M. A. Shestopalov, G. F. Chimonides, P. Mikes, P. D. Topham, S. J. Kim, N. Kitamura and A. J. Sutherland, Photoluminescent Materials Based on PMMA and a Highly-Emissive Octahedral Molybdenum Metal Cluster Complex, *J. Mater. Chem. C*, 2016, **4**(3), 497–503.
35 M. N. Sokolov, M. A. Mihailov, E. V. Peresypkina, K. A. Brylev, N. Kitamura and V. P. Fedin, Highly Luminescent Complexes [Mo6X8(n-C3F7COO)(6)][2-) (X = Br, I), *Dalton Trans.*, 2011, **40**(24), 6375–6377.
36 K. Kirakci, S. Cordier and C. Perrin, Synthesis and Characterization of $Cs_2Mo_6X_{14}$ (X = br or 1) Hexamolybdenum Cluster Halides: Efficient Mo-6 Cluster Precursors for Solution Chemistry Syntheses, *Z. Anorg. Allg. Chem.*, 2005, **631**(2–3), 411–416.
37 D. M. Kroupa, J. Y. Roh, T. J. Milstein, S. E. Creutz and D. R. Gamelin, Quantum-Cutting Ytterbium-Doped $CsPb(Cl_{1-x}Br_x)(3)$ Perovskite Thin Films with Photoluminescence Quantum Yields over 190%, *ACS Energy Lett.*, 2018, **3**(10), 2390–2395.
38 R. R. Lunt, Theoretical Limits for Visibly Transparent Photovoltaics, *Appl. Phys. Lett.*, 2012, **101**(4), 043902.
39 C. J. Traverse, R. Pandey, M. C. Barr and R. R. Lunt, Emergence of Highly Transparent Photovoltaics for Distributed Applications, *Nat. Energy*, 2017, **2**(11), 849–860.
40 T. J. Milstein, D. M. Kroupa and D. R. Gamelin, Picosecond Quantum Cutting Generates Photoluminescence Quantum Yields Over 100% in Ytterbium-Doped $CsPbCl_3$ Nanocrystals, *Nano Lett.*, 2018, **18**(6), 3792–3799.
41 C. C. Yang, D. Y. Liu and R. R. Lunt, How to Accurately Report Transparent Luminescent Solar Concentrators, *Joule*, 2019, **3**(12), 2871–2876.
42 L. R. Bradshaw, K. E. Knowles, S. McDowall and D. R. Gamelin, Nanocrystals for Luminescent Solar Concentrators, *Nano Lett.*, 2015, **15**(2), 1315–1323.
43 R. Mazzaro, A. Gradone, S. Angelon, G. Morselli, P. G. Cozzi, F. Romano, A. Vomiero and P. Ceroni, Hybrid Silicon Nanocrystals for Color-Neutral and Transparent Luminescent Solar Concentrators, *ACS Photonics*, 2019, **6**(9), 2303–2311.
44 F. Meinardi, A. Colombo, K. A. Velizhanin, R. Simonutti, M. Lorenzon, L. Beverina, R. Viswanatha, V. I. Klimov and S. Brovelli, Large-Area Luminescent Solar Concentrators Based on 'Stokes shift-Engineered' Nanocrystals in a

Mass-Polymerized PMMA Matrix, *Nat. Photonics*, 2014, **8**(5), 392–399.

45 J. Choi, D. Nguyen, E. Gi, K. A. Brylev, J. W. Yu, D. Kim, W. B. Lee, D. H. Kim, I. Chung, K. K. Kim and S. J. Kim, A highly efficient and transparent luminescent solar concentrator based on a nanosized metal cluster luminophore anchored on polymers, *J. Mater. Chem. C*, 2022, **10**(11), 4402–4410.